THE JOURNAL OF BIOLOGICAL CHEMISTRY Vol. 277, No. 36, Issue of September 6, pp. 33325–33333, 2002
Printed in U.S.A.

Intracellular Trafficking and Membrane Targeting Mechanisms of the Human Reduced Folate Carrier in Mammalian Epithelial Cells*[S]

Received for publication, June 14, 2002
Published, JBC Papers in Press, June 26, 2002, DOI 10.1074/jbc.M205955200

Jonathan S. Marchant‡§¶, Veedamali S. Subramanian¶‖‡‡, Ian Parker‡, and Hamid M. Said‖**‡‡¶¶**

*From the Departments of ‡Neurobiology and Behavior, ‖Medicine, and **Physiology and Biophysics, University of California, Irvine, California 92697, the §Department of Pharmacology, University of Minnesota, 55455, and the ‡‡Department of Veterans Affairs Medical Center, Long Beach, California 90822*

The major pathway for cellular uptake of the water-soluble vitamin folic acid in mammalian cells is via a plasma membrane protein known as the reduced folate carrier (RFC). The molecular determinants that dictate plasma membrane expression of RFC as well as the cellular mechanisms that deliver RFC to the cell surface remain poorly defined. Therefore, we designed a series of fusion proteins of the human RFC (hRFC) with green fluorescent protein to image the targeting and trafficking dynamics of hRFC in living epithelial cells. We show that, in contrast to many other nutrient transporters, the molecular determinants that dictate hRFC plasma membrane expression reside within the hydrophobic backbone of the polypeptide and not within the cytoplasmic NH_2- or COOH-terminal domains of the protein. Further, the integrity of the hRFC backbone is critical for export of the polypeptide from the endoplasmic reticulum to the cell surface. This trafficking is critically dependent on intact microtubules because microtubule disruption inhibits motility of hRFC-containing vesicles as well as final expression of hRFC in the plasma membrane. For the first time, these data define the mechanisms that control the intracellular trafficking and cell surface localization of hRFC within mammalian epithelia.

Folate is necessary for the synthesis of precursors of nucleic acids, initiation of protein synthesis in mitochondria, and metabolism of certain amino acids (1, 2). Deficiency of this essential micronutrient leads to a variety of abnormalities including derangement of one-carbon metabolism and inhibition of growth. Humans and other mammals do not possess the ability to synthesize folate and must obtain this vitamin from exogenous sources by intestinal absorption. Absorption occurs from both dietary sources in the small intestine and from bacterially synthesized folate in the large intestine (3, 4). Thereafter, folate is distributed into different body compartments where it is taken up by individual cell types for use in different metabolic reactions. Many previous studies have shown that the main folate uptake pathway in cells occurs via a specialized carrier-mediated mechanism, the reduced folate carrier (RFC[1]; in humans, known as hRFC) (4–6). The RFC is also involved in intestinal absorption of folate from the small and large intestine (5). The functional properties of this transport pathway have been well characterized (4–6) and its molecular identity established after cloning of its cDNA (7–9) and characterization of its flanking regulatory regions (4).

In contrast, comparatively little is known about the mechanisms that control the intracellular trafficking of the RFC protein and its appropriate expression in the plasma membrane, topics of particular importance for transport of folate by mammalian epithelial cells. Genetic defects in such folate transport processes have been reported previously; however, little is known about the exact sites of these defects (10). To address these questions, we used high resolution confocal imaging techniques to monitor the distribution and transport of hRFC fusion proteins tagged with the enhanced green fluorescent protein (EGFP) in living mammalian epithelial cell lines. By comparing the expression patterns of nine truncated hRFC mutants, we show that targeting of hRFC to the plasma membrane depends on the integrity of the membrane-spanning "backbone" of the protein, rather than on targeting sequences in the NH_2- or COOH-terminal cytoplasmic regions. Furthermore, by using video-rate confocal microscopy, we resolved the intracellular trafficking dynamics of hRFC-containing vesicles and demonstrate that delivery of hRFC-EGFP to the cell surface is critically dependent on intact microtubules but not microfilaments. Taken together, these results highlight how the hRFC polypeptide sequence is targeted and delivered to the cell surface within a physiologically relevant context, and they define the regions of the hRFC protein in which mutations would impair folate transport by disrupting trafficking and targeting mechanisms.

EXPERIMENTAL PROCEDURES

Materials—FM4-64 was from Molecular Probes (Eugene, OR). Green (EGFP-N3) and yellow (EYFP-membrane) fluorescent protein vectors were from BD Biosciences (Palo Alto, CA). Cytochalasin D, nocodazole, colchicine, and γ-lumicolchicine were from Calbiochem. Tissue culture cell lines were obtained from ATCC (Manassas, VA). All other reagents were obtained from Sigma or from suppliers outlined previously (11, 12).

* This work was supported by the Department of Veterans Affairs, the University of Minnesota Medical School, and National Institutes of Health Grants DK-56061 and DK-58057 (to H. M. S.) and GM-48071 (to I. P.). The costs of publication of this article were defrayed in part by the payment of page charges. This article must therefore be hereby marked "*advertisement*" in accordance with 18 U.S.C. Section 1734 solely to indicate this fact.

[S] The on-line version of this article (available at www.jbc.org) contains Videos 1–4.

¶ Both authors contributed equally to this work.

¶¶ To whom correspondence should be addressed. Tel.: 562-826-5811; Fax: 562-826-5731; E-mail: hmsaid@uci.edu.

[1] The abbreviations used are: RFC, reduced folate carrier; hRFC, human reduced folate carrier; EGFP, enhanced green fluorescent protein; EYFP, enhanced yellow fluorescent protein; HEK, human embryonic kidney.

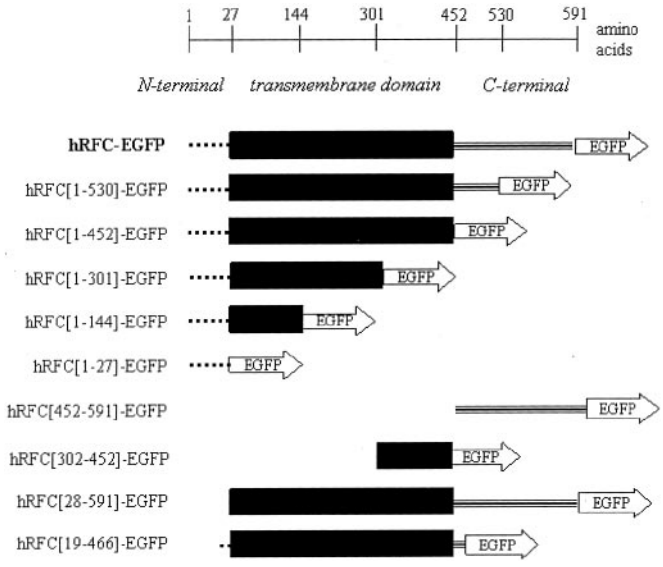

FIG. 1. **Construction of hRFC-EGFP fusion proteins.** A schematic representation of the amino acid sequence of the full-length hRFC-EGFP fusion protein (*top*) together with nine truncated fusion constructs (*bottom*) is shown. Regions containing the NH_2-terminal cytoplasmic region (residues 1–27, *dotted line*), transmembrane backbone (*black bar*), and COOH-terminal cytoplasmic tail (residues 452–591, *striped line*) are indicated relative to the sequence of full-length hRFC. In each construct EGFP was fused to the COOH terminus of the protein.

Construction of hRFC-EGFP and Truncated Constructs—cDNA encoding the open reading frame of the full-length hRFC and various truncated constructs (Fig. 1) were generated by PCR using the primer sequences and combinations shown in Table I. PCRs were carried out as described previously (11), and the resulting products were gel isolated and ligated together with the EGFP coding sequence digested from the EGFP-N3 vector. This method generated in-frame fusion proteins under the control of the human cytomegalovirus promoter. The nucleotide sequence of each resulting construct was confirmed by sequencing (SeqWright, Houston, TX and Laragen, Inc., CA).

Cell Culture and Transient Transfection—Human embryonic kidney (HEK-293) cells, human duodenal derived intestinal epithelial (HuTu-80) cells, and Madin-Darby canine kidney cells were maintained in minimum Eagle's medium containing 10% fetal bovine serum. Human colon adenocarcinoma (Caco-2) cells were maintained in Dulbecco's modified Eagle's medium (20% fetal bovine serum) and human colonic (NCM 460) cells in Ham's F-12 medium (20% fetal bovine serum). All media contained glutamine, sodium bicarbonate, penicillin, and streptomycin. For transient transfection, cells were grown on poly-D-lysine-coated cover slips cemented in holes at the bottom of sterile Petri dishes (MatTek, MA) and were transfected at ~90% confluence with plasmid DNA complexes using LipofectAMINE 2000 (Invitrogen). For all transfection protocols, conditions were optimized to minimize the amount of DNA used (typically ~0.6 μg of cDNA of the indicated construct and less than recommended by the manufacturers) to minimize any nonspecific effects of fusion protein overexpression. Monolayers were subsequently imaged using confocal microscopy at indicated times after transfection (typically ~48 h).

Confocal Imaging of hRFC Constructs—Cell monolayers were monitored for hRFC-EGFP expression using a custom built laser scanning confocal microscope (12) or a video-rate scanning confocal microscope (13). Both instruments were based on Olympus IX70 inverted microscopes fitted with 40×, NA 1.35 oil immersion objectives. EGFP, EYFP, DsRed, and FM4-64 were all excited using the 488 nm line from an argon ion laser, and emitted fluorescence was monitored using a 530 ± 20 nm band pass filter (EGFP, EYFP) or 650LP filter (DsRed, FM4-64). For slow frame scanning, confocal images were obtained by scanning either laterally (top view; *x-y* scans) or axially (side view; *x-z* scans) across the specimen.

For video-rate imaging experiments, images were recorded at 30 Hz (one frame every 33 ms) from confocal sections with the microscope focused about 2 μm above the coverglass within cells maintained at 22 or 37 °C. Data were digitized using the stream acquisition function of the Metamorph processing package (Universal Imaging, Downingtown, PA). The resulting image stacks (*x-y* time) were then smoothed using a two-frame average to yield a final image stack at 66-ms frame intervals. The motions of individual vesicles were tracked using the point-to-point tracking function in Metamorph, and the resulting paths were exported to the Origin graphing package for analysis. QuickTime videos of image sequences are appended as supplementary material.

Flow Cytometry—HEK-293 cells were used for these experiments because their high (~40%) efficiency of transfection allowed counting of large cell populations (15,000 cells for each construct, three experiments). Monolayers of HEK-293 cells were transfected *in situ* within individual T75 tissue culture flasks using ~4 μg of cDNA encoding individual constructs. Cells were trypsinized and resuspended in Ca^{2+}-free phosphate-buffered saline, and populations of >15,000 transfected cells were measured for intensity of fluorescence emission (488 nm excitation, 530 ± 15 nm emission) using a FACStation fluorescence analysis system (Becton Dickinson Immunocytometry Systems).

RESULTS

Cellular Distribution of hRFC-EGFP—To visualize the targeting of hRFC in mammalian cells, we transiently transfected a variety of epithelial cell lines with cDNA encoding the full-length fusion construct (hRFC-EGFP) and analyzed the resulting fluorescence distribution by confocal microscopy. In HuTu-80 cells (human duodenal epithelium), hRFC-EGFP expression was evident at the cell surface and in cellular processes extending from the cell membrane as well in a population of discrete, intracellular vesicular structures (Fig. 2*A*, see also later). This distribution of fluorescence contrasted markedly with HuTu-80 cells expressing EGFP alone, in which the entire cytosolic volume was fluorescent (Fig. 2*B*). These contrasting distributions were also evident in axial (*x-z*) sections of cells expressing hRFC-EGFP (Fig. 2*C*) or EGFP alone (Fig. 2*D*), which suggested that hRFC-EGFP was targeted to all plasma membrane domains of the cell. The localization of hRFC-EGFP to the plasma membrane was not unique to HuTu-80 cells because a similar targeting was evident from lateral (*x-y*) sections images in a variety of other mammalian epithelial cell lines including HEK-293, Caco-2, Madin-Darby canine kidney, and NCM-460 cells (Fig. 2*E*).

Identification of Polypeptide Domains Important for hRFC Expression and Targeting—To determine the domains within the hRFC protein which are important for its correct trafficking and targeting we compared the cellular distribution seen with the full-length hRFC-EGFP with that observed with the series of hRFC mutants diagrammed in Fig. 1.

Fig. 3 shows representative lateral confocal images of HuTu-80 cells transiently transfected with each of the indicated constructs and imaged 48 h later when the full-length hRFC-EGFP was almost completely distributed to the plasma membrane (see below). It is apparent that changes in the sequence of hRFC resulted in a wide variety of cellular distributions. Four classes of distribution were evident: 1) expression primarily at the cell surface (hRFC[1–530]-EGFP, hRFC[1–452]-EGFP, and hRFC[19–466]-EGFP, Fig. 3*A*); 2) cytosolic, non-membrane-bound expression (hRFC[452–591]-EGFP and hRFC[1–27]-EGFP, Fig. 3*B*); 3) expression confined within intracellular membranes (hRFC[1–301]-EGFP and hRFC[1–144]-EGFP, Fig. 3*C*); 4) a heterogeneous distribution, spanning several of the above categories (hRFC[28–591]-EGFP and hRFC[302–452]-EGFP, Fig. 3*D*). Expression of hRFC[28–591]-EGFP was evident at the cell surface as well as throughout the intracellular compartments, whereas hRFC[302–452]-EGFP was restricted to intracellular membranes soon after transfection and thereafter appeared in the cytoplasm. This latter profile is suggestive of a poorly tolerated protein structure that is actively targeted for degradation (14).

To quantify the relative amounts of hRFC protein expressed in the plasma membrane *versus* that in other cellular compartments, we imaged transfected cells that were costained by

TABLE I

Combination of primers used for preparation of the different constructs by PCR

Table 1 shows the sequence and combination of primers used for the preparation of the different constructs by PCR. Restriction sites for *BamHI* (boldface text) and *XhoI* (underlined) were added to specific hRFC primers to assist cloning into the pEGFP-N3 vector.

Construct	Forward and reverse primers (5′ → 3′)	Position	Fragment
		bp	*bp*
hRFC-EGFP	CCG**CTCGAG**ATGGTGCCCTCCAGCCCAGCG; CGGGATCCCTGGTTCACATTCTGAACACCG	1–1773	1773
hRFC[1–530]-EGFP	CCG**CTCGAG**ATGGTGCCCTCCAGCCCAGCG; CGGGATCCGGCCGGGGCCTGGGCCAG	1–1590	1590
hRFC[1–452]-EGFP	CCG**CTCGAG**ATGGTGCCCTCCAGCCCAGCG; CGGGATCCCAGCATGGCCCCCAAGAAGTAG	1–1356	1356
hRFC[1–301]-EGFP	CCG**CTCGAG**ATGGTGCCCTCCAGCCCAGCG; CGGGATCCACTGTTGGTGGTGGGGTCCA	1–903	903
hRFC[1–144]-EGFP	CCG**CTCGAG**ATGGTGCCCTCCAGCCCAGCG; CGGGATCCCACGAGAGAGAAGATGTAGGAGGAA	1–432	432
hRFC[1–27]-EGFP	CCG**CTCGAG**ATGGTGCCCTCCAGCCCAGCG; CGGGATCCGCGCCGCCAGGACCG	1–81	81
hRFC[452–591]-EGFP	CCG**CTCGAG**ATGGATGGCCTGCGGCACTGC; CGGGATCCCTGGTTCACATTCTGAACACCG	1356–1773	417
hRFC[302–452]-EGFP	CCG**CTCGAG**ATGGCGCGGGTCTACAACGG; CGGGATCCCAGCATGGCCCCCAAGAAGTAG	904–1356	453
hRFC[28–591]-EGFP	CCG**CTCGAG**ATGCTCGTGTGCTACCTTTGCTTC; CGGGATCCCTGGTTCACATTCTGAACACCG	82–1773	1692
hRFC[19–466]-EGFP	CCG**CTCGAG**ATGGACCCCGAGCTCCGGT; CGGGATCCCTGCCGCGGGTGGTGG	54–1398	1344

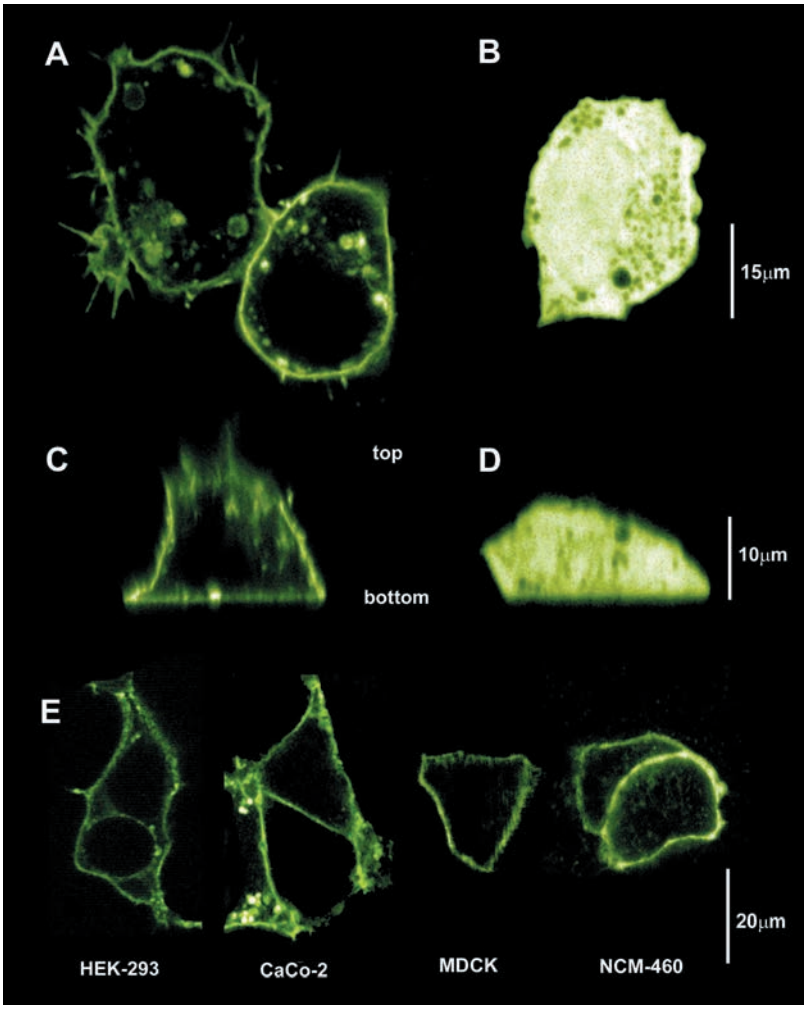

FIG. 2. **Distribution of hRFC-EGFP in epithelial cells.** *A*, confocal images (*x*-*y*) showing two adjacent HuTu-80 cells expressing hRFC-EGFP, imaged 48 h after transient transfection. *B*, fluorescence distribution in a HuTu-80 cell transfected with EGFP alone. *C* and *D*, axial confocal sections (*x*-*z*) of the same HuTu-80 cells shown in *A* and *B*, expressing hRFC-EGFP (*C*) or EGFP alone (*D*). *E*, distribution of hRFC-EGFP in a variety of different mammalian epithelial cell lines, each imaged 48 h after transient transfection.

extracellular application of the red emitting lipophilic dye FM4-64 (15). This selectively labels the plasma membrane, thereby allowing us to estimate the extent of localization of hRFC-EGFP at the cell surface by measuring the degree of overlap of red and green fluorescence. Examples are shown in Fig. 3*E* for cells expressing hRFC-EGFP at the cell surface (high degree of overlap with FM4-64: *yellow* color) and cells expressing a construct (hRFC[1–301]-EGFP) that remained localized to intracellular membranes (little fluorescence colocalization).

Fig. 3*F* shows measurements of fluorescence colocalization obtained in this way for the various constructs. A high degree (>50%)

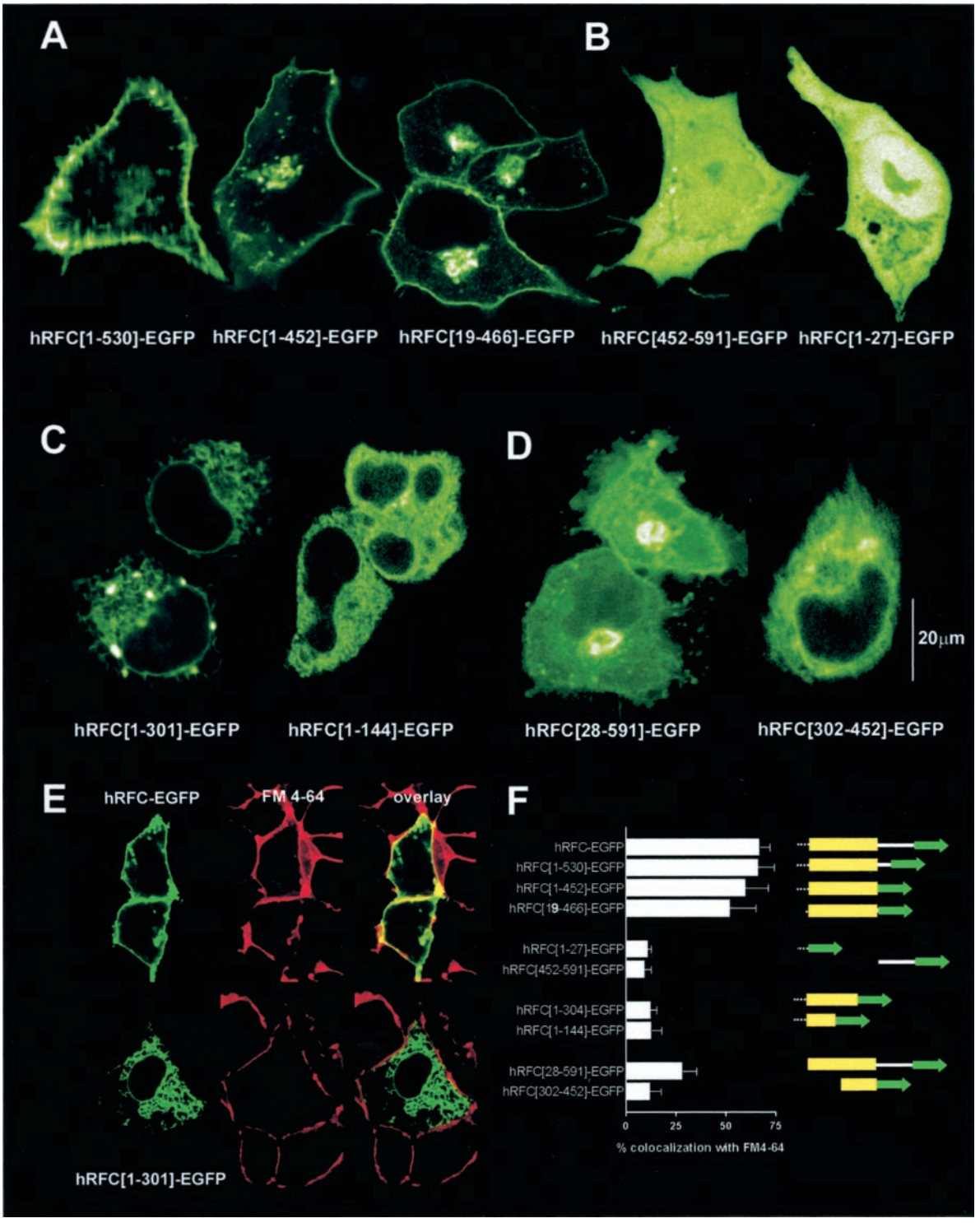

FIG. 3. **Cellular distribution of hRFC constructs in HuTu-80 cells.** The montage shows a series of representative lateral (*x-y*) confocal sections from HuTu-80 cells transfected 48 h previously with the indicated constructs. The laser power was adjusted individually to obtain final images of equivalent brightness, and these do not therefore reflect differences in efficiency of protein expression among the constructs. Constructs are grouped into categories (*A–D*) as described under "Experimental Procedures." *E*, colocalization of EGFP and FM4-64 fluorescence as a method of quantifying the extent of expression of different hRFC constructs at the plasma membrane. Images illustrate HuTu-80 cells transfected with hRFC-EGFP (*top*) and hRFC[1–301]-EGFP (*bottom*). *Panels* on the *left* were obtained using a green band pass filter to show only EGFP fluorescence. *Panels* in the *middle* were obtained using a red long pass filter to show distribution of the red fluorescent dye FM4-64 in the plasma membrane. The *right panels* show overlays of the *red* and *green* images, with regions of colocalization appearing *yellow*. *F*, bar graphs showing values of colocalization between FM4-64 and EGFP fluorescence for each of the indicated constructs. Schematic diagrams on the *right* illustrate the structures of each construct (NH_2 terminus, *white dotted line*; transmembrane domain, *yellow bar*; COOH terminus, *white line*; GFP, *green arrow*). Data are the mean of values from ≥20 cells.

of colocalization was seen in cells expressing hRFC-EGFP, hRFC[1–530]-EGFP, hRFC[1–452]-EGFP, and hRFC[19–466]-EGFP, confirming that these four constructs targeted efficiently to the cell surface. Little colocalization (~8–14%, equivalent to that (~10%) with EGFP alone) was seen with hRFC[1–301]-EGFP, hRFC[1–144]-EGFP, hRFC[1–27]-EGFP, hRFC[452–591]-EGFP,

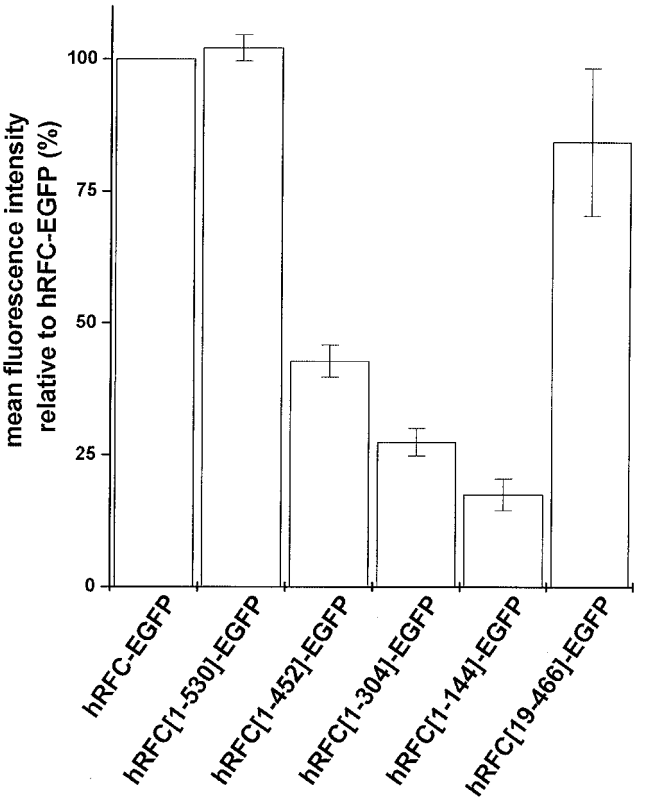

FIG. 4. **Efficiency of expression of hRFC-EGFP with different constructs.** Histogram bars show the mean total fluorescence of HEK-293 cells transfected with different constructs, expressed as a percentage of that obtained with the full-length hRFC-EGFP construct and measured on a flow cytometer (mean of at least three independent experiments).

and hRFC[302–452]-EGFP, confirming their inability to target to the cell surface. An intermediate degree of colocalization (~ 28%) was seen with hRFC[28–591]-EGFP, suggesting that a small proportion of the expressed construct was delivered to the cell surface.

In addition to the differing cellular localization of hRFC-EGFP proteins expressed by the different constructs, it was also apparent that the total amount of protein expressed varied greatly among constructs. For example, although hRFC-EGFP and hRFC[1–452]-EGFP were both expressed selectively at the cell surface, cells expressing the latter construct were much dimmer (at equivalent laser power) than hRFC-EGFP-transfected cells. Given identical transfection conditions (0.6 μg of DNA, imaged after 48 h) and promoter expression, this variability presumably reflects differences in cellular processing for each construct (*e.g.* relative rates of protein synthesis and degradation). To quantify these differences, we used flow cytometry to measure the distributions of total fluorescence of cells transfected with constructs that showed predominant targeting to the plasma membrane (hRFC-EGFP, hRFC[1–530]-EGFP, hRFC[1–452]-EGFP, hRFC[19–466]-EGFP) or to intracellular membranes (hRFC[1–301]-EGFP and hRFC[1–144]-EGFP). HEK-293 cells were used for these experiments because their high transfection efficiency permitted measurements from large (>15,000) populations of cells. We note however, that the subcellular distribution of each hRFC construct was identical in both HEK-293 and HuTu-80 cell lines (Fig. 2*C* and data not shown).

Fig. 4 shows that although the level of protein expression was not reduced appreciably by either partial truncation of the COOH-terminal cytoplasmic tail (mean fluorescence of the hRFC[1–530]-EGFP population 102 ± 3% of that of hRFC-EGFP, three independent runs) or by partial truncation of both the COOH-terminal and NH_2-terminal regions (hRFC[19–466]-EGFP, 84 ± 14%), complete truncation of the COOH-terminal hRFC-EGFP sequence substantially decreased the level of expression (hRFC[1–452]-EGFP, 42.7 ± 3%). Further truncations into the hRFC backbone reduced expression further (hRFC[1–301]-EGFP, 27.4 ± 3% and hRFC[1–144]-EGFP, 17.5 ± 3%). Taken together, the data of Figs. 3 and 4 show that the hRFC structure dictates the subcellular targeting as well as the efficiency of protein expression within mammalian cells.

Trafficking of hRFC-EGFP Involves Microtubule-based Transport—In contrast to other membrane transporters (16–18), little is known about the cytoskeletal mechanisms that direct the intracellular trafficking of hRFC (11). To resolve this issue, we examined the possible roles of microfilaments and microtubules in transporting hRFC-EGFP to the cell surface by using pharmacological methods to disrupt the cytoskeleton selectively.

To identify an appropriate time window for pharmacological intervention, we began by characterizing the kinetics of hRFC-EGFP expression after transfection. Fluorescence was initially apparent after 4 h as a weak juxtanuclear signal. Subsequently, the fluorescence increased, spread throughout the cell, and became increasingly localized to the plasma membrane (Fig. 5*A*). The relative extent of hRFC-EGFP expression at the cell surface was estimated by costaining with FM4-64, as before. At early times after transfection (~ 4–5 h) there was little colocalization between hRFC-EGFP distribution and FM4-64 staining (12.1 ± 2.5%, Fig. 5, *B left* and *C*), and this value was similar to that with EGFP alone (16.7 ± 6%; Fig. 5*C*). However, by 36 h colocalization between hRFC-EGFP and FM4-64 had increased to a maximal value (63.5 ± 6%, Fig. 5, *B right* and *C*) as a result of trafficking of hRFC-EGFP to the cell surface, whereas colocalization in cells transfected with EGFP alone (9.1 ± 6%) or hRFC[1–304]-EGFP (13.8 ± 9%, ≥15 cells) failed to show any further increase (Fig. 5*C*).

As shown in Fig. 5*C*, hRFC-EGFP fluorescence at the cell surface began to increase rapidly about 12 h after transfection, and we thus selected this as a suitable time point at which to apply cytoskeletal disrupting drugs, either cytochalasin D, a microfilament disrupting agent, or nocodazole, a microtubule-disrupting agent. Both drugs were added to the incubation medium at final concentrations (400 nM) that are sufficient to disrupt cytoskeletal architecture but minimize toxicity during the prolonged (8 h) application (11, 20). Colocalization of FM4-64 and hRFC-EGFP fluorescence was then assessed 8 h later (*i.e.* 20 h after transfection). Measurements are shown in Fig. 5*D*, expressed as the change in colocalization relative to that measured at 12 h to reflect trafficking of hRFC-EGFP to the plasma membrane during the time the drugs were present. Although colocalization of fluorescence between hRFC-EGFP and FM4-64 increased to a similar extent in untreated cells (2.2 ± 0.4-fold, n = 12 cells) and cells treated with cytochalasin D (2.0 ± 0.3-fold, n = 21 cells), a slight decrease was seen after incubation with nocodazole (0.91 ± 0.42-fold, n = 39 cells). Thus, disruption of the microtubular cytoskeleton almost completely inhibited hRFC-EGFP trafficking to the plasma membrane, whereas disruption of the actin cytoskeleton was without effect.

Transport Dynamics of hRFC-containing Vesicles—Confocal images of hRFC-EGFP distribution in HuTu-80 cells revealed numerous intracellular vesicular-like structures (Figs. 2*A* and 6*A*). To measure the dynamics of these structures and further investigate the role of cytoskeletal elements in hRFC transport, we employed video-rate confocal imaging to capture image sequences with sufficient temporal resolution to track move-

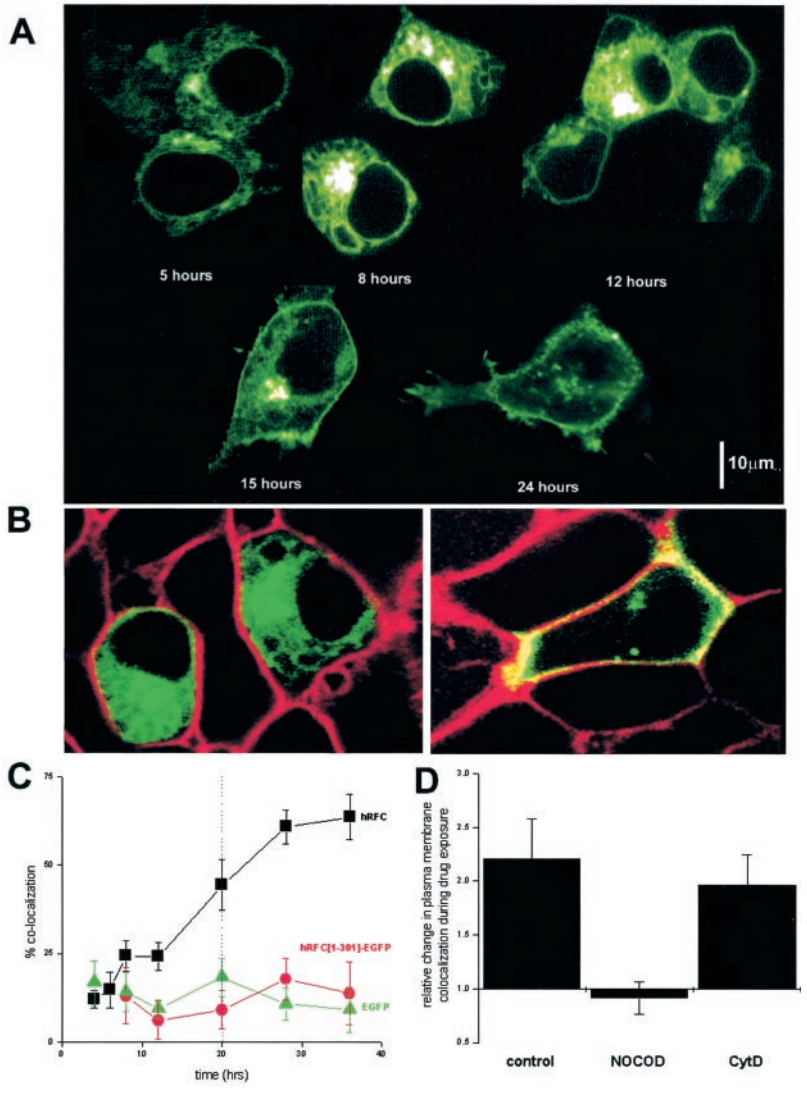

FIG. 5. **Effect of cytoskeletal disruption on delivery of hRFC-EGFP to the plasma membrane.** *A*, distribution of hRFC-EGFP in HEK-293 cells imaged at different times after transfection with the full-length construct. *B*, dual color overlay of confocal images of hRFC-EGFP-expressing HEK-293 cells obtained 5 h (*left*) and 30 h (*right*) after transfection. The distribution of hRFC-EGFP is shown in *green*, and the plasma membrane was labeled in *red* by the lipophilic dye FM4-64. Overlap (colocalization) between these two labels is depicted in *yellow*. *C*, relative distribution of various EGFP constructs in the plasma membrane, assayed by colocalization of the green fluorescence with the red membrane marker, as illustrated in *B*. Separate culture dishes of HEK-293 cells were transfected with hRFC-EGFP (*black squares*), EGFP alone (*green triangles*), or hRFC[1–301]-EGFP (*red circles*), and colocalization was measured at various times after transfection. Each point is a mean from ≥10 cells. *D*, effect of cytoskeletal disruption on hRFC-EGFP expression at the cell surface. Cytochalasin D or nocodazole (both at 400 nM) were added to cells 12 h after transfection, and the colocalization between hRFC-EGFP and FM4-64 fluorescence was estimated subsequently after 20 h (*dotted blue line* in *C*). Values represent the relative change in cell surface expression of hRFC-EGFP over this period (*i.e.* 1 = no change). Control measurements (hRFC-EGFP) are shown from culture dishes imaged in parallel which were not treated with drug.

ments of individual vesicles. Experiments were performed at both 37 °C (Fig. 6*A*) and 22 °C (Fig. 6*B*), and results under both conditions are displayed in Fig. 6 as well as in the supplemental video material (Videos 1 and 2). Fig. 6*A* shows a single frame from a video collected at 37 °C (*left*) and illustrates the method used to track the motion of hRFC-EGFP-containing structures (*right*). The coordinates of discrete fluorescent structures were tracked at 66-ms intervals (two-frame averages) to generate color-coded tracks representing movements of several vesicles throughout the imaging period (Fig. 6*A*, *right*). Fig. 6*B* shows similar processing applied to a cell maintained at 22 °C from which several tracks have been expanded to illustrate generalized aspects of hRFC-EGFP dynamics.

Four general features were evident from cells incubated at both temperatures. First, hRFC-EGFP was localized within structures of varied size and shape (diameters ~0.3–1.6 μm), including spherical as well as tubular-like vesicles (Videos 1 and 2). Second, there was a wide variability in the dynamics of hRFC-containing vesicles. Some showed little motion (*e.g.* vesicle *a*, Fig. 6*B*), whereas others remained highly dynamic over the entire imaging period or displayed interspersed periods of relatively static and dynamic behavior (*e.g.* vesicle *b*, Fig. 6*B*). Third, the motion of dynamic vesicles was strikingly multidirectional rather than showing unidirectional progression toward the plasma membrane. Vesicles frequently retraced their paths, moved toward and away from the cell surface (*e.g.* vesicle *d*, Fig. 6*B*) or tracked circumferentially beneath the plasma membrane (*e.g.* vesicle *c*, Fig. 6*B*). Finally, vesicles located within the same portion of the cell often showed significant overlap in their tracks (examples in Fig. 6, *A–C*).

The high temporal resolution of these video-rate confocal images revealed two discrete components to the observed vesicular dynamics, namely, periods of rapid, approximately linear motion (*e.g.* regions marked by *black lines* for vesicle *b*, Fig. 6*B*), interspersed with lengthy periods of relative immobility during which vesicles displayed Brownian-like movements constrained within a small area (Fig. 6*B*). These alternating patterns of motion were apparent at both temperatures, but at 22 °C the dwell time of vesicles in the stationary state became longer, and their velocities during linear motions were slower (Fig. 6*C*). Further reduction in temperature to 4 °C almost completely inhibited motility (data not shown).

To quantitate the effect of temperature better, we measured the velocities of vesicles during periods of rapid, directed linear transport. Measurements at 37 °C from 79 vesicles (15 cells) showed linear movement over a mean distance (run length) of 3.16 ± 0.16 μm at a velocity of 1.56 ± 0.22 μm s^{-1} compared with an average velocity of 0.66 ± 0.07 μm s^{-1} over a linear distance of 2.99 ± 0.42 μm at 22 °C (Fig. 6*D*). Further, the dwell time at rest was 70.4 ± 3.6% at 22 °C, decreasing to 49.8 ± 5.1% at 37 °C (125 vesicles, ≥9 cells, Fig. 6*D*).

Having determined these parameters under control conditions, we proceeded to examine the effect of cytoskeletal disruption on vesicle motion. Video data were recorded before and

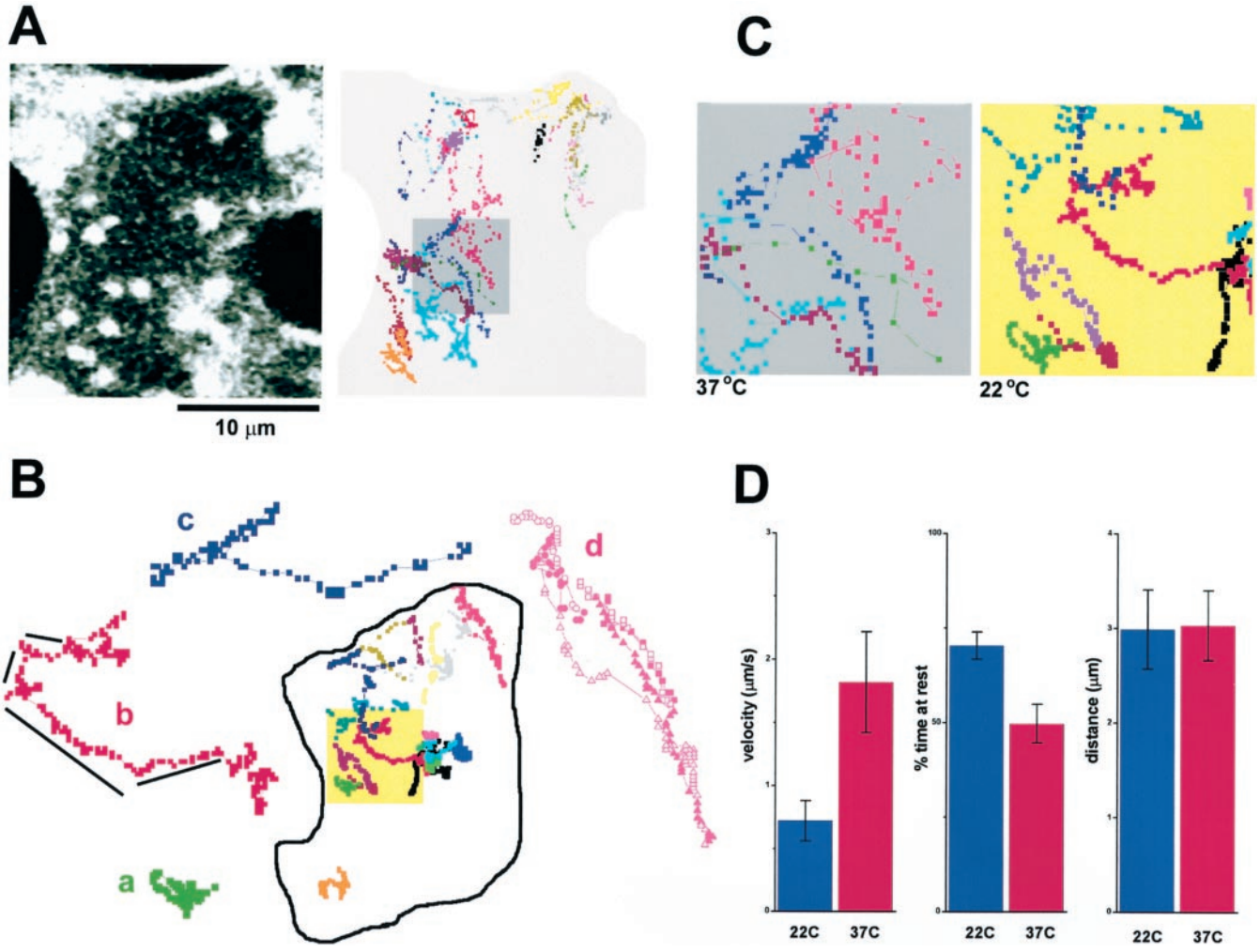

FIG. 6. **Vesicular dynamics of hRFC-EGFP resolved by video-rate confocal imaging.** *A*, *left*, average of two consecutive video confocal frames, showing the distribution of hRFC-EGFP-containing vesicles close to the basal membrane of a HuTu-80 cell maintained at 37 °C. The video sequence from which this image was obtained is available as supplementary material (Video 1). *Right*, tracks of individual vesicles (represented by different *colors*) derived from the video. *B*, tracks from a HuTu-80 cell at 22 °C. Individual tracks (*a*, *b*, *c*, and *d*, identified by *colors*) are shown expanded to illustrate examples of a relatively static vesicle (*a*), a vesicle exhibiting rapid linear movements (*lines*) interspersed with periods of immobility (*b*), a vesicle showing lateral movements beneath the plasma membrane (*c*), and a vesicle undergoing multiple changes in direction highlighted by changes in symbol at successive reversals (*c*). *C*, expanded regions (~6 μm square) from indicated areas in *A* and *B* to illustrate point-to-point vesicular motion at 37 °C (*left*) and 22 °C (*right*). Points are plotted every 200 ms (every three data points). *D*, graphs show mean velocities during linear motions (*left*), percentage of time at rest (*middle*), and run lengths (*right*) of vesicles in cells maintained at 37 °C (*red*) and 22 °C (*blue*). Data are from >50 vesicles in ≥11 cells.

after addition of the microtubule disrupting drugs nocodazole (10 μM) or colchicine (10 μM), with γ-lumicolchicine (100 μM) as a negative control, and the actin-disrupting agent cytochalasin D (10 μM). Videos were taken at 5-min intervals after drug addition, and vesicular dynamics during linear motions were analyzed as above. Observation of cells for up to 30 min (30-s imaging periods every 5 min) showed that exposure to the laser scan had little deleterious effect on vesicular dynamics (average velocities at the start and end of the 30 min recording were 1.82 ± 0.4 μm s^{-1} *versus* 1.65 ± 0.4 μm s^{-1}, respectively; ≥8 cells, Fig. 7*A*). In contrast, incubation of cells with 10 μM nocodazole inhibited the linear motion of vesicles within 5 min (n = 15 cells, Fig. 7, *A* and *B*). Colchicine had a similar effect, albeit over a slower time course. After a 5-min incubation in 10 μM colchicine, the linear motion of vesicles had decreased to 0.66 ± 0.07 μm/s (from 11 cells), and by 20 min motion was inhibited (Fig. 7*A*). γ-Lumicolchicine, even at concentrations as high as 100 μM for 30 min, failed to inhibit vesicular motility (linear velocity of 1.69 ± 0.23 μm/s, Fig. 7*A*). Similarly, the actin-destabilizing drug cytochalasin D was without effect on the velocity (1.47 ± 0.22 μm/s; 15 cells) of linear vesicular movement (Fig. 7, *A* and *C*). Representative tracks from cells treated with nocodazole and cytochalasin D are shown, respectively, in Fig. 7, *B* and *C*, and the videos from which they are derived are available as supplemental material (Videos 3 and 4).

DISCUSSION

In this study, we employed confocal imaging methods to answer three questions regarding the cell biology of hRFC. Where is the full-length hRFC-EGFP fusion protein localized in mammalian epithelial cells? How does the sequence of the hRFC protein control its cellular targeting? What cellular mechanism(s) underlie the trafficking of hRFC to the cell membrane? Our results in each of these areas are discussed separately below.

Cellular Localization of hRFC-EGFP—Ligation of the green fluorescent protein to the COOH terminus of the full-length hRFC sequence generates a functional fusion protein (11, 21) that we had shown previously localizes to the plasma membrane of *Xenopus* oocytes (11). Here we extended those studies to mammalian cells and show that hRFC-EGFP similarly targets to the plasma membrane of a human duodenally derived

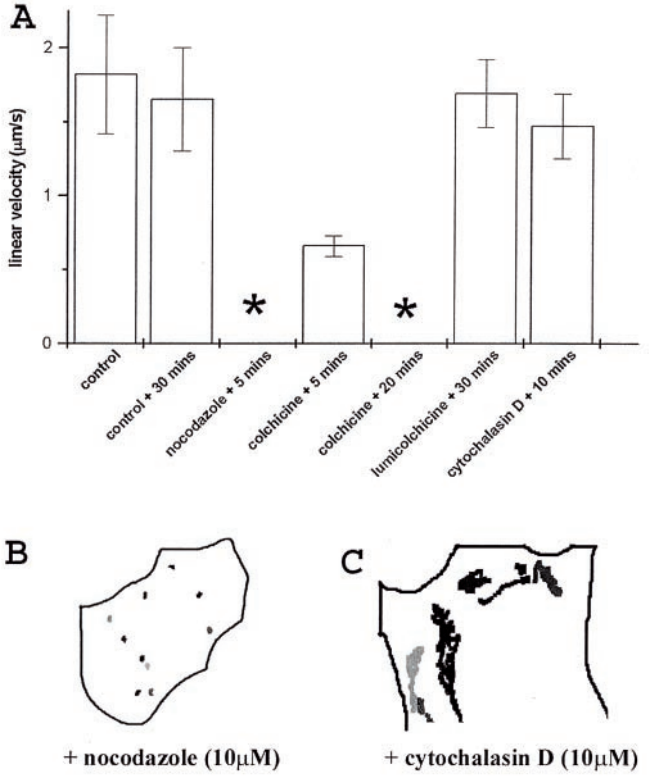

FIG. 7. **Effect of cytoskeletal drugs on dynamics of hRFC-containing vesicles.** *A*, velocities of hRFC-EGFP-containing vesicles measured at various times after the addition of 10 μM nocodazole, 10 μM colchicine, 100 μM γ-lumicolchicine, and 10 μM cytochalasin D. *Bars* show mean velocities (>20 vesicles in ≥5 cells), measured during rapid, linear movements, at 37 °C. *Asterisks* indicate cases in which vesicle movements were too small to compute velocities. *B* and *C*, representative vesicle tracks in cells treated, respectively, with 10 μM nocodazole for 5 min and 10 μM cytochalasin D for 5 min. Videos from which these tracks were derived are available as supplemental material (Videos 3 and 4, respectively).

cell line (HuTu-80; Fig. 2, *A* and *C*) as well as several other epithelial cell lines (Fig. 2*E*). However, in addition to hRFC-EGFP expressed at the plasma membrane, intracellular structures also showed appreciable fluorescence (Figs. 2, 3, 6, and 7). The proportion of fluorescent protein in intracellular structures was greatest soon after transfection and likely represents biosynthetic and trafficking pools of hRFC-EGFP. Nevertheless, about 30% of cellular hRFC-EGFP was retained intracellularly (Fig. 6*C*) even >30 h post-transfection. The identity of these intracellular structures and the possibility that they are in exchange with the plasma membrane compartment are being investigated currently.

Confocal images of the axial distribution of hRFC-EGFP in HuTu-80 monolayers (*e.g.* Fig. 2*C*) indicate that hRFC-EGFP targets to the entire cell surface rather than showing a strongly asymmetric distribution across the cell. These data suggest that folate transport can occur over the entire cell surface, consistent with previous results from *in vitro* assays (22, 23). However, it is important to state that the targeting of membrane proteins to specific cell surface domains is likely dependent on the culture conditions as well as cell type (24–26), and our results should be considered only in that context and may not, therefore, reflect the polarity of hRFC distribution *in vivo*.

Molecular Determinants of hRFC Targeting in Mammalian Cells—We show that the polypeptide domains essential for targeting hRFC to the plasma membrane reside within the polypeptide backbone of the protein rather than in the NH_2-terminal (amino acids 1–27) or COOH-terminal (amino acids 452–591) cytoplasmic portions of the protein. Partial or full truncation of the cytoplasmic tail of hRFC (hRFC[1–530]-EGFP and hRFC[1–452]-EGFP, respectively) did not affect the plasma membrane targeting of these constructs (Fig. 3). Similarly, ablation of the NH_2-terminal sequence (hRFC[28–591]-EGFP) did not prevent cell surface localization. Further, the doubly truncated construct (hRFC[19–466]-EGFP), with ablation of both the NH_2-terminal and COOH-terminal tails, still localized to the plasma membrane (Fig. 3).

Although the NH_2- and COOH-terminal cytoplasmic regions are nonessential for conferring cell surface localization, these regions play accessory roles in modulating the efficiency of expression. For example, although the NH_2-terminal-deleted construct (hRFC[28–591]-EGFP) reached the cell surface, a considerable portion of this protein was retained intracellularly (Fig. 3). Further, measurements of the total fluorescence intensity showed differences that likely relate to their expression level (Fig. 4). Fluorescence intensity decreased on full (hRFC[1–452]-EGFP), but not partial (hRFC[1–530]-EGFP), truncation of the COOH-terminal cytoplasmic tail (Fig. 4). This consideration could be of clinical significance in that truncation mutations (14) may affect not only the function and trafficking of hRFC to the cell surface, but also the rates of synthesis and degradation of the mutated proteins. Finally, we note that in the *Xenopus* oocyte expression system hRFC-EGFP, hRFC[1–530]-EGFP and hRFC[1–452]-EGFP targeted to the plasma membrane in a similar manner to that in HuTu-80 cells, with hRFC[1–452]-EGFP again being expressed at a similarly lower efficiency (11). Thus, the targeting mechanisms of hRFC appear well conserved among very different cell types and organisms.

A third important point is that the integrity of the backbone of hRFC-EGFP is important for export of the polypeptide from the endoplasmic reticulum to the cell surface. Proteins in which the COOH-terminal end of the polypeptide backbone was truncated (hRFC[1–301]-EGFP and hRFC[1–144]-EGFP) remained trapped within intracellular membranes (Fig. 3). Similarly, truncation of the NH_2-terminal end of the polypeptide backbone (hRFC[302–452]-EGFP), resulted in low expression and intracellular localization. Because the constructs hRFC[1–301]-EGFP and hRFC[302–452]-EGFP, taken together, comprise the entire sequence of hRFC-EGFP, this suggests that no single contiguous amino acid motif dictates export to the cell surface. Rather, a more complex interplay between two or more determinants distributed widely along the polypeptide backbone appears to be involved.

Sequences critical for plasma membrane targeting have been identified in many different cell surface proteins. In contrast to our findings with hRFC, such motifs frequently reside within the cytoplasmic NH_2- or COOH-terminal tails of these proteins (27–32). For example, truncation of the COOH-terminal tails of the rat liver-rat Na^+/bile acid cotransporter (29), the type iib NaP_i cotransporter (31), or the NH_2-terminal domain of the SGLT1 glucose transporter prevents cell surface expression of the respective proteins (28). However, these cytoplasmic regions seem to play a less essential role in directing the cell surface targeting of hRFC. This observation is not without precedent within the major facilitator superfamily of transporters (33) because similar results have been obtained with other proteins that share the 12 membrane-spanning topology of hRFC (21). For example, the COOH-terminal tail is not essential for cell surface targeting, stability, or function of the *Escherichia coli* H^+/lactose permease (34), and total truncation of the COOH-terminal tail of the glucose transporter GLUT1 impaired function, but not cell surface localization (35). However, it is probably unwise to generalize about conserved tar-

geting mechanisms among different classes of proteins, especially because of the low sequence similarity between the RFC family and other transporters within this group. Our data simply underscore the plethora of targeting signals that can act to route polypeptides to their final cellular destinations.

Intracellular Trafficking of hRFC-EGFP—Our previous studies (11) involving expression of hRFC in *Xenopus* oocytes indicated that delivery of hRFC-EGFP to the plasma membrane involves microtubule based transport. Here, we confirm that finding in mammalian epithelial cells and describe the subcellular dynamics of this vesicular transport process.

First, the microtubule-disrupting agent nocodazole almost completely abolished cell surface expression of hRFC-EGFP, whereas disruption of actin filaments by cytochalasin D was without effect. Second, measurements of the dynamics of hRFC-containing vesicles yielded velocities ($\sim$1.2–1.5 μm s^{-1}) and linear run lengths (average of $\sim$3 μm, ranging up to $\sim$8 μm) consistent with values reported for microtubule-based vesicular motion in a variety of other cell types (36, 37) and with the speeds of the microtubule-based motors kinesin and dynein measured *in vitro* (38). For example, microtubule-based transport of GLUT4 vesicles in adipocytes (albeit resolved at $\sim$10-fold slower frame rates) occurs with linear velocities of $\sim$0.8 μm s^{-1} over distances of 5–9 μm (39). Similarly, microtubule-dependent velocities of exocytotic vesicles in Chinese hamster ovary cells were measured to be $\sim$1 μm s^{-1} with run lengths of $\sim$3 μm (36). Finally, nocodazole rapidly inhibited the rapid, linear movements of hRFC-EGFP-containing vesicles (Fig. 7). This effect was mimicked by colchicine but not γ-lumicolchicine, a non-tubulin-binding analog (19). Actin-destabilizing drugs were without effect (Fig. 7).

A strikingly feature was that movement of hRFC-EGFP-containing vesicles was multidirectional. Individual vesicles displayed an apparent haphazard pattern of motion, frequently retracing their steps, despite the net progression of protein to the cell surface. This behavior likely results because association with microtubules is only transient and is interrupted by breaks, with subsequent directional changes on reassociation with individual microtubules (Fig. 6*B*). Such multidirectional transport, and especially, rapid reversal of individual vesicles on single tracks, supports roles for both plus end- and minus end-directed motors attached to individual hRFC-EGFP-containing vesicles (36). Further, our observation of frequent circumferential movements close to the cell surface suggests that the final stage of insertion, and possibly retrieval, of hRFC-EGFP from the cell membrane may be a precisely regulated process.

In summary, our results demonstrate that the molecular determinants responsible for hRFC targeting to the cell surface of mammalian epithelia are integral to the hydrophobic backbone of the polypeptide, rather than lying within the NH_2- and COOH-terminal cytoplasmic regions. Further, the integrity of the backbone of hRFC is essential for export of the protein from the endoplasmic reticulum and its trafficking via microtubules to the cell surface.

Acknowledgments—We thank Arsalan Hejazi for help with data analysis.

REFERENCES

1. Blakley, R. L., and Whitehead, V. A. (1986) *Folates and Pterins: Nutritional, Pharmacological and Physiological Aspects*, John Wiley and Sons, New York
2. Titus, S. A., and Moran, R. G. (2000) *J. Biol. Chem.* **275,** 36811–36817
3. Said, H. M., and Kumar, C. (1999) *Curr. Concepts Gastroenterol.* **15,** 172–176
4. Sirotnak, F. M., and Tolner, B. (1999) *Annu. Rev. Nutr.* **19,** 91–122
5. Said, H. M., Rose, R., and Seetharam, B. (2000) in *Gastrointestinal Transport Molecular Physiology* (Barritt, K. E., and Donowitz, M., eds) pp. 35–75, Academic Press, San Diego
6. Mason, J. B., and Rosenberg, I. H. (1994) in *Physiology of the Gastrointestinal Tract* (Johnson, L. R., ed) Vol. 2, pp. 1979–1996, Raven Press, New York
7. Moscow, J. A., Gong, M., He, R., Sgagias, M. K., Dixon, K. H., Anzick, S. L., Mettzer, P. S., and Cowan, K. H. (1995) *Cancer Res.* **55,** 3790–3794
8. Nguyen, T. T., Dyer, D. L., Dunning, D. D., Rubin, S. A., Grant, K. E., and Said, H. M. (1997) *Gastroenterology* **112,** 783–791
9. Wong, S. C., Proefke, S. A., Bhusan, A., and Matherly, L. H. (1995) *J. Biol. Chem.* **270,** 17468–17475
10. Geller, J., Kronn, D., Jayabose, S., and Sandoval, C. (2002) *Medicine* (*Baltimore*) **81,** 516–568
11. Subramanian, V. S., Marchant, J. S., Parker, I., and Said, H. M. (2001) *Am. J. Physiol.* **281,** G1477–G1486
12. Parker, I., Callamaras, N., and Wier, W. G. (1997) *Cell Calcium* **21,** 441–452
13. Callamaras, N., and Parker, I. (1999) *Cell Calcium* **26,** 271–279
14. Sadlish, H., Murray, R. C., Williams, F. M. R., and Flintoff, W. F. (2000) *Biochem. J.* **346,** 509–518
15. Janecki, A. J., Janecki, M., Akhter, S., and Donowitz, M. (2000) *J. Histochem. Cytochem.* **48,** 1479–1481
16. Achler, C., Filmer, D., Mertre, C., and Drenckhahn, D. (1989) *J. Cell Biol.* **109,** 179–189
17. Caplan, M. J. (1997) *Am. J. Physiol.* **272,** F425–F429
18. Brown, D. (2000) *Am. J. Physiol.* **278,** F192–F201
19. Goldschmide, R. B., and Steward, O. (1989) *Brain Res.* **486,** 133–140
20. Grigoriev, I. S., Chernobelskaya, A. A., and Vorobjev, I. A. (1999) *Membr. Cell Biol.* **13,** 23–48
21. Ferguson, P. L., and Flintoff, W. F. (1999) *J. Biol. Chem.* **23,** 16269–16278
22. Said, H. M., Ghishan, F. K., and Redha, R. (1987) *Am. J. Physiol.* **252,** G229–G236
23. Dudeja, P. K., Kode, A., Alnounou, M., Tyagi, S., Torania, S., Subramanian, V. S., and Said, H. M. (2001) *Am. J. Physiol.* **281,** G54–G60
24. Roush, D. L., Gottardi, C. J., Naim, H. Y., Roth, M. G., and Caplan, M. J. (1998) *J. Biol. Chem.* **273,** 26862–26869
25. Sweet, D. H., Miller, D. S., and Pritchard, J. B. (2000) *Am. J. Physiol.* **279,** F826–F834
26. Karim-Jimenez, Z., Hernando, N., Biber, J., and Murer, H. (2001) *Pflügers Arch.* **442,** 782–790
27. Ammon, C., Schafer, J., Kreuzer, O. J., and Meyerhof, W. (2002) *Arch. Physiol. Biochem.* **110,** 137–145
28. Suzuki, T., Fujikura, K., Koyama, H., Matsuzaki, T., Takahashi, Y., and Takata, K. (2001) *Eur. J. Cell Biol.* **80,** 765–774
29. Sun, A.-Q., Arrese, M. A., Zeng, L., Swaby, I., Zhou, M. M., and Suchy, F. J. (2001) *J. Biol. Chem.* **276,** 6825–6833
30. Jacob, R., Alfalah, M., Grunberg, J., Obendorf, M., and Naim, H. Y. (2000) *J. Biol. Chem.* **275,** 6566–6572
31. Karim-Jimenez, Z., Hernando, N., Biber, J., and Murer, H. (2000) *Proc. Natl. Acad. Sci. U. S. A.* **97,** 2916–2921
32. McCarthy, J. B., Lim, S. T., Elkind, B., Trimmer, J. S., Duvoisin, R. M., Rodriguez-Boulan, E., and Caplan, M. J. (2001) *J. Biol. Chem.* **276,** 9133–9140
33. Goswitz, V. C., and Brokker, R. J. (1995) *Protein Sci.* **4,** 534–537
34. Roepe, P. D., Zbar, R. I., Sarkar, H. K., and Kaback, H. R. (1989) *Proc. Natl. Acad. Sci. U. S. A.* **86,** 3992–3996
35. Due, A. D., Zhi-Chao, Q., Thomas, J. M., Buchs, A., Powers, A. C., and May, J. M. (1995) *Biochemistry* **34,** 5462–5471
36. Trinczek, B., Ebneth, A., Mandelkow, E. M., and Mandelkow, E. (1999) *J. Cell Sci.* **112,** 2355–2367
37. Hollinshead, M., Rodger, G., Van Eijl, H., Law, M., Hollinshead, R., Vaux, D. J. T., and Smith, G. L. (2001) *J. Cell Biol.* **154,** 389–402
38. Hirokawa, N. (1998) *Science* **279,** 519–526
39. Fletcher, L. M., Welsh, G. I., Oatey, P. B., and Tavare, J. M. (2000) *Biochem. J.* **352,** 267–276